Transient structural distortion of metal-free Cu/Zn superoxide dismutase triggers aberrant oligomerization

Kaare Teilum[a,b], Melanie H. Smith[a,1], Eike Schulz[a,2], Lea C. Christensen[b], Gleb Solomentsev[a], Mikael Oliveberg[c], and Mikael Akke[a,3]

[a]Center for Molecular Protein Science, Biophysical Chemistry, Lund University, SE-22100 Lund, Sweden; [b]Structural Biology and NMR Laboratory, Department of Biology, University of Copenhagen, DK-2200 Copenhagen, Denmark; and [c]Department of Biochemistry and Biophysics, The Arrhenius Laboratories for Natural Sciences, Stockholm University, SE-10691 Stockholm, Sweden

Edited by Alan Fersht, University of Cambridge, Cambridge, UK and approved August 31, 2009 (received for review July 2, 2009)

Amyotrophic lateral sclerosis (ALS) is a neurodegenerative disease linked to the misfolding of Cu/Zn superoxide dismutase (SOD1). ALS-related defects in SOD1 result in a gain of toxic function that coincides with aberrant oligomerization. The structural events triggering oligomerization have remained enigmatic, however, as is the case in other protein-misfolding diseases. Here, we target the critical conformational change that defines the earliest step toward aggregation. Using nuclear spin relaxation dispersion experiments, we identified a short-lived (0.4 ms) and weakly populated (0.7%) conformation of metal-depleted SOD1 that triggers aberrant oligomerization. This excited state emanates from the folded ground state and is suppressed by metal binding, but is present in both the disulfide-oxidized and disulfide-reduced forms of the protein. Our results pinpoint a perturbed region of the excited-state structure that forms intermolecular contacts in the earliest nonnative dimer/oligomer. The conformational transition that triggers oligomerization is a common feature of WT SOD1 and ALS-associated mutants that have widely different physicochemical properties. But compared with WT SOD1, the mutants have enhanced structural distortions in their excited states, and in some cases slightly higher excited-state populations and lower kinetic barriers, implying increased susceptibility to oligomerization. Our results provide a unified picture that highlights both (*i*) a common denominator among different SOD1 variants that may explain why diverse mutations cause the same disease, and (*ii*) a structural basis that may aid in understanding how different mutations affect disease propensity and progression.

amyotrophic lateral sclerosis | nuclear magnetic resonance relaxation | protein misfolding

Amyotrophic lateral sclerosis (ALS) is a motor neuron disease with an incidence of 1–2 per 100,000 and a lifetime risk of 1/1,000 that results in paralysis and respiratory failure, typically within 1–5 years of onset (1). The most common familial form of ALS has been linked to Cu/Zn superoxide dismutase (SOD1) (2), a 32-kDa homodimeric antioxidant enzyme (Fig. 1*A*). Transgenic mice models have shown that mutations in SOD1 can induce ALS through a gain of cytotoxic function (3, 4), the molecular basis of which remains unknown. The prevailing hypothesis, based on the accumulation of insoluble protein deposits in motor neurons, asserts that pathogenesis involves protein misfolding and aggregation (1, 2). Mounting evidence indicates that the gain of toxic function in SOD1-linked ALS, as in many other misfolding diseases, is caused by molecular species that arise early in the aggregation process as opposed to the macroscopic deposits per se (5–8). The structural events triggering oligomerization have remained enigmatic, however, as is the case in other protein-misfolding diseases (9). A detailed view of the misfolding and oligomerization pathway involving SOD1 is of fundamental importance for elucidating the molecular basis of ALS.

Monomeric metal-free (apo) SOD1 is a pertinent starting point for addressing the initial events causing aberrant oligomerization. SOD1 undergoes complex posttranslational maturation, including formation of the intramolecular C57–C146 disulfide bond, binding of Zn, chaperone-assisted insertion of Cu, and dimerization (10, 11). However, several lines of evidence indicate that it is apo-SOD1, not the metal-bound states, that plays a key role in aberrant oligomerization (11–19). In vitro studies of the aggregation kinetics have implicated the monomeric apo state as the origin for aggregation (12–14). In addition, partially misfolded and monomeric SOD1 has been detected in ALS mouse models (20) and in vivo–like erythrocyte systems (21). The relative population of apo monomers is expected to be higher for mutations that adversely affect metal binding or dimerization of SOD1 (2). It also is known that reduction of the C57-C146 disulfide promotes dissociation of the native dimer (11, 22), but contrasting data have been reported regarding the role of intermolecular disulfide bonds in the aggregation of SOD1 (8, 15, 16, 23, 24). Previous reports have identified a flexible region in monomeric apo-SOD1, including the metal-binding loops and neighboring β-sheet, which has been suggested as the primary candidate for forming an aggregation-prone interface (18, 19, 25).

Based on these insights, we set out to characterize the critical process that turns innocuous SOD1 into an aggregation-prone species. We used Carr-Purcell-Meiboom-Gill (CPMG) ^{15}N nuclear spin relaxation experiments, which are capable of detecting minute quantities of short-lived excited states against the dominant background of ground-state protein (26, 27). CPMG experiments yield the rate of exchange between the ground state and the excited state, together with the relative populations of these states and the NMR frequency (chemical shift) difference between them, which is a sensitive indicator of structural changes. Thus, the experiments determine the kinetics and thermodynamics of the conformational transition and also provide structural information on the excited state.

Author contributions: K.T., M.H.S., M.O., and M.A. designed research; K.T., M.H.S., E.S., L.C.C., and G.S. performed research; K.T. and M.O. contributed new reagents/analytic tools; K.T., M.H.S., E.S., G.S., and M.A. analyzed data; and K.T., M.H.S., and M.A. wrote the paper.

The authors declare no conflict of interest.

This article is a PNAS Direct Submission.

Data deposition: Backbone chemical shift assignments for WT apo-SOD1 and mutants A4V, G85R, and D90A have been deposited at the BioMagResBank, www.bmrb.wisc.edu (accession nos. 15711, 15712, 15713, and 15714).

[1]Present address: Department of Cellular and Molecular Pharmacology, University of California, 1700 4th Street, San Francisco, CA 94158.

[2]Present address: Department of Molecular Structural Biology, University of Göttingen, Justus-von-Liebig-Weg 11, 37077 Göttingen, Germany.

[3]To whom correspondence should be addressed. E-mail: mikael.akke@bpc.lu.se.

This article contains supporting information online at www.pnas.org/cgi/content/full/0907387106/DCSupplemental.

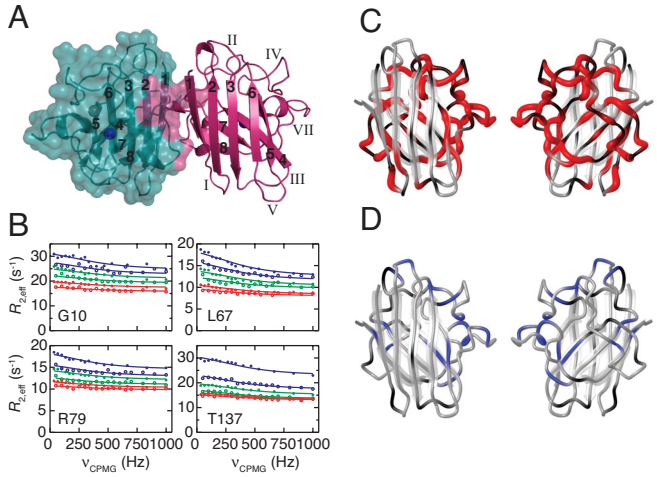

Fig. 1. Transient structural distortion of monomeric WT SOD1. (*A*) Structure of the native Cu/Zn-bound SOD1 dimer (35). Green and magenta ribbons represent the two molecules. The solvent-accessible surface is outlined in green, and the dimer interface is colored magenta. The Cu (blue) and Zn (green) ions are indicated. β-strands are numbered 1–8 and loops I–VII. (*B*) Representative ^{15}N CPMG relaxation dispersions (R_2^{eff} vs. ν_{CPMG}) recorded at 2 static magnetic fields (open symbols, 50.6 MHz; filled symbols, 60.8 MHz) and 3 temperatures (blue, 18 °C; green, 25 °C; red, 32 °C). The solid lines represent the global fit to a 2-state process. (*C*) Residues with perturbed structure in the excited state of apo-SOD1 are shown in red. The tube width encodes $\Delta\omega_{FE}$ = 354-1720 s^{-1}. Black denotes prolines and residues lacking data due to spectral overlap; gray denotes residues not showing relaxation dispersion. Left-side view: as for the right-side molecule in (*A*); right-hand view: rotated by 180° around the vertical axis. (*D*) Residues showing quantifiable exchange in Zn-SOD1 are colored blue; in other respects, the layout follows (*C*). The global fit yielded k_{ex} = 22 ± 1 s^{-1} and $\langle\Delta\omega_{AB}\rangle$ = (14 ± 9) × 10 s^{-1}.

More than 100 different mutations in SOD1 have been linked to familial ALS, but how the great variation in molecular properties (e.g., stability and metal affinity) among these mutants relate to the same disease is not well understood (2, 28). To investigate this issue, we studied both WT SOD1 and 4 familial ALS mutants. The mutants were selected based on their well-established links to familial ALS and their diverse physicochemical properties. The monomeric apo states of A4V, G85R, and G93A are all highly destabilized toward global unfolding, whereas D90A imparts only a marginal effect in this respect (14). G85R and D90A have a lower net negative charge, which increases the aggregation propensity (14, 28), and G85R has a lower metal affinity, which increases the relative population of apo-SOD1 (2). A4V and G93A confer short survival times in patients with ALS (< 3 years), while G85R and D90A are associated with more variable disease progression (1, 2). Here, we report a transient structural distortion that triggers oligomerization of monomeric apo-SOD1. Our dynamics profiling of these SOD1 variants offers physicochemical and structural insights that may explain mutation-specific variations in disease propensity.

Results

Apo-SOD1 Undergoes a Reversible Conformational Transition. We measured ^{15}N CPMG relaxation dispersion profiles on WT apo-SOD1 at 3 different temperatures. A total of 64 backbone nitrogen nuclei showed measurable exchange contributions to the transverse relaxation rate. The relaxation dispersions from these residues at all 3 temperatures were fit globally to a 2-state exchange process (Fig. 1*B*, Figs. S1 and S2, and Table S1). The results reveal that WT apo-SOD1 exchanges reversibly between the folded ground state (F) and an excited state (E) that has a relative population of p_E = 0.7% (Fig. 1 *B* and *C* and Table 1). The rate of exchange between the folded and excited states, k_{ex} = 2.2 × 10^3 s^{-1}, is 5 and 7 orders of magnitude faster than the rates of global folding and unfolding, respectively (14), demonstrating that the excited state is located on the folded side of the major folding barrier.

Table 1. Parameters describing the transient structural transition in WT and mutant variants of apo-SOD1 at 25° C and pH 6.3

Variant	k_{ex} (×10^3 s^{-1})	p_E (%)	n*
WT†	2.2 ± 0.1	0.7 ± 0.1	64
A4V	3.0 ± 0.3	1.0 ± 0.5	39
G85R	3.9 ± 0.6	1.1 ± 0.6	31
D90A	3.6 ± 0.3	1.2 ± 0.3	68

*Number of residues included in the fit.
†The parameters for WT apo-SOD1 were obtained from a global fit to data acquired at 3 temperatures: 18° C, 25° C, and 32° C. The global fit also included the enthalpy difference between the folded and excited states, ΔH_{FE} = −57 ± 5 kJ/mol. From p_E and ΔH_{FE}, the differences in free energy and entropy are obtained: ΔG_{FE} = 12.1 ± 0.2 kJ/mol and ΔS_{FE} = −0.22 ± 0.01 kJ/mol/K.

The temperature dependence of the relaxation dispersion data reflects the energy landscape of SOD1. The global fit included the enthalpy difference between the folded and excited states, ΔH_{FE} = −57 ± 5 kJ/mol. Together with p_E, this yields the free energy and entropy differences, ΔG_{FE} = 12.1 ± 0.2 kJ/mol and ΔS_{FE} = −0.22 ± 0.01 kJ/mol/K. Thus, formation of the excited state is enthalpically favorable, but entropically unfavorable.

To visualize the structural difference between the folded and excited states of apo-SOD1, we mapped those residues that exhibit relaxation dispersion onto the structure of apo-SOD1 (Fig. 1*C*). Extensive regions of the 8-stranded β-sandwich are perturbed in the excited state, including the flexible loops IV, VI, and VII and the β-sheet formed by strands β4, β5, β7, and β8. In contrast, the sheet formed by strands β1–3 and β6 remains largely unaffected in the excited state (Fig. 1*C*). Structural perturbations are not observed for the ground state, which has well-folded β-sheets as gauged from ^{15}N longitudinal relaxation rates and {^{1}H}–^{15}N NOE measurements (25).

Structural analysis shows that the peptide backbone of residues A60, G61, P62, H63, and F64 populates 2 distinct conformations related to *cis*/*trans* isomerization of the G61–P62 peptide bond. The chemical shift of P62 $^{13}C^{\beta}$ identifies the sets of resonances arising from the *cis* and *trans* conformations (29), and the corresponding peak intensities indicate that the relative populations are ≈25% and ≈75%, respectively. Notably, the excited state emanates exclusively from the major *trans* isomer, while the *cis* isomer shows no conformational exchange (Fig. S3).

To investigate whether the observed exchange process relates to unfolding of the affected segments, we compared the magnitude of the chemical shift differences between the folded and excited states, $\Delta\omega_{FE}$ (extracted from the CPMG data), to the changes in chemical shift expected for complete unfolding, $\Delta\omega_{FU}$ (30) (Fig. S4). There is no correlation between $\Delta\omega_{FE}$ and $\Delta\omega_{FU}$ (Pearson's r = −0.14), indicating that the observed conformational exchange does not involve complete unfolding of these segments. In fact, $\Delta\omega_{FE}$ is greater than $\Delta\omega_{FU}$ in the loops IV and VII, which have small values of $\Delta\omega_{FU}$, possibly suggesting that these regions are more structured in the excited state than in the ground state.

The C57-C146 Disulfide Does Not Control Excited State Formation. CPMG data acquired on the disulfide-reduced form of WT apo-SOD1 revealed conformational exchange for 13 residues in the same regions as in the oxidized state, with p_E = 0.6% and k_{ex} = 3.4 × 10^3 s^{-1} (Fig. S5*A*). Thus, the population of the excited

state in disulfide-reduced and disulfide-oxidized apo-SOD1 is the same within the limits of experimental error, whereas the rate of exchange is slightly faster in the reduced state than in the oxidized state. The low number of residues that show exchange in reduced apo-SOD1 is a consequence of the faster exchange rate, which renders the CPMG dispersions measurable only for residues with large $\Delta\omega_{FE}$. The residues for which we observe exchange in reduced apo-SOD1 thus correspond to those that have the largest $\Delta\omega_{FE}$ in the oxidized state. In conclusion, the oxidation state of the disulfide does not appear to control the excited state formation in monomeric apo-SOD1, in agreement with computational studies of local unfolding in apo-SOD1 (17), but might modulate the lifetime of the excited state.

Conformational Exchange Is Suppressed in Zn-SOD1. We verified that the excited state is a unique feature of apo-SOD1 by performing complementary CPMG experiments on Zn-bound SOD1 (Zn-SOD1) (Fig. S5*B*). In contrast to apo-SOD1, Zn-SOD1 does not undergo any large-scale conformational exchange. Eighteen residues in the regions around the Zn binding site and the superoxide access channel show evidence of slow conformational exchange with small structural changes (compare Fig. 1 *C* and *D*). These distinct differences in conformational integrity explain why apo-SOD1 forms oligomeric structures, whereas Zn-SOD1 does not (11, 15).

Transient Intermolecular Contacts Are Identified by Paramagnetic Relaxation. We mixed ^{15}N-labeled SOD1 with non–isotope-labeled SOD1 that had been tagged with the paramagnetic spin label methanethiosulfonate (MTSL), which causes a strongly distance dependent relaxation enhancement (31). Significant paramagnetic relaxation enhancement (PRE) is observed (Figs. 2*A* and S6), establishing that monomeric apo-SOD1 forms transient intermolecular interactions. The observed pattern of PRE across the protein structure differs significantly from that expected for the native apo dimer (Fig. 2 *A*–*C*); for example, sizeable PREs are observed for residues H80 and V81, whose backbone amides are buried in the interior of the ground-state protein, as well as for residues L67, S68, and R69, which shield H80 and V81 from the solvent and are located 6–10 Å away from these residues. These observations indicate that the PREs are due to nonnative dimers or higher-order oligomers, and that intermolecular contacts occur between species that have undergone significant structural rearrangements. Most importantly, PREs are observed only for the *trans*-(G61-P62) conformer (Fig. 2*D*), directly mirroring the CPMG results. Consequently, apo-SOD1 must be in the *trans*-(G61-P62) conformation to (*i*) reach the excited state and (*ii*) form oligomers. Together, the PRE and CPMG results strongly indicate that oligomerization occurs specifically via the excited state. Because the observed exchange parameters are independent of concentration (Fig. S7), we conclude that the excited state is predominantly monomeric, but forms oligomers in a transient fashion.

Familial ALS Mutants of SOD1 Show Enhanced Perturbations. We investigated whether the structural transition occurs for ALS-associated SOD1 mutants as well and, if so, whether these affect the transition process or the structure of the excited state. We performed ^{15}N CPMG relaxation measurements on 4 ALS mutants: A4V, G85R, D90A, and G93A (Figs. 3*A* and S8). The ^{1}H-^{15}N correlation spectra of WT and A4V, G85R, and D90A show very similar structures (Fig. S9). In contrast, G93A is predominantly (≈90%) unfolded under the same conditions, as expected due to its low stability (14). The unfolded state of G93A does not exhibit conformational exchange on the millisecond time scale, in keeping with the conclusion that the excited state of apo-SOD1 is located on the folded side of the major folding barrier. The low population of folded G93A precluded CPMG

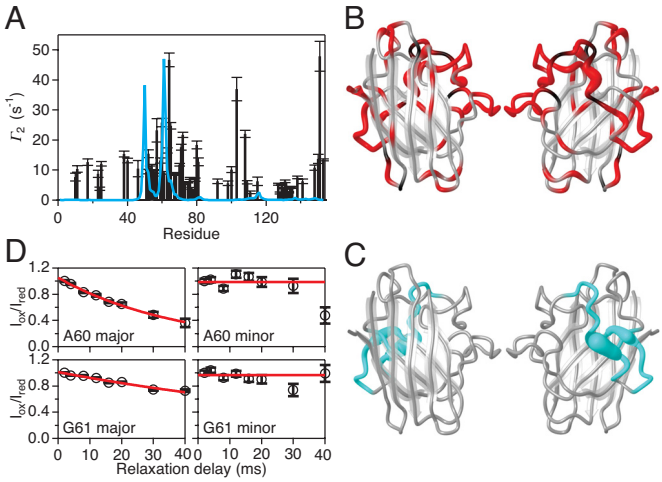

Fig. 2. Transient oligomerization in the excited state of WT apo-SOD1. (*A*) PRE, Γ_2, of transverse ^{1}H magnetization in WT apo-SOD1 in the presence of the spin-labeled apo-SOD1 variant Q153C-MTSL. The measured Γ_2 is plotted versus residue number (black bars), with estimated errors indicated. The blue line shows the Γ_2 profile expected for transient formation of the native dimer (3%). (*B*) Residues in WT apo-SOD1 with significant Γ_2 ($P < 0.01$) are shown in red. The width of the worm diagram indicates the magnitude of Γ_2, which scales with r^{-6}, where r is the distance from the spin label in the nonnative dimer or oligomer. Black denotes prolines and residues lacking data due to spectral overlap; gray denotes residues that do not experience significant Γ_2. (*C*) Calculated values of $\Gamma_2 > 2$ s^{-1} expected for transient formation of the native dimer are shown in blue [corresponding to the blue line in (*A*)]. (*D*) Representative experimental data showing PRE decays for A60 and G61 in the major and minor conformations of WT apo-SOD1 that are due to *cis-trans* isomerization around the G61–P62 peptide bond. The relative cross-peak intensity measured in MTSL-oxidized and MTSL-reduced samples is plotted versus the relaxation delay. The fitted values are $\Gamma_2 = 25.9 \pm 1.4$ s^{-1} for A60 and 9.1 ± 0.5 s^{-1} for G61.

measurements for this state. For the remaining 3 mutants, the CPMG results reveal the existence of a conformational transition similar to that detected in WT apo-SOD1 (Table 1 and Fig. 3). Although k_{ex} and p_E for the mutants are close to the values measured for the WT, statistical analysis indicates that the differences are significant ($P < 0.05$), except for the p_E of A4V (Table S2). To this extent, both k_{ex} and p_E tend to be slightly increased for the mutants compared with WT.

The residue-specific values of $\Delta\omega_{FE}$ for the mutants correlate with the values measured for WT SOD1 (Fig. 3 *E* and *F*), demonstrating that the excited state has a similar overall structure in the different variants. Focusing next on the detailed chemical shift patterns, we pinpoint residues that have an altered structure in the excited state of the mutants but apparently remain unaffected in WT (Fig. 3 *B*–*D*). We defer any further interpretations of potential differences in $\Delta\omega_{FE}$ between variants until future work that includes additional nuclei (e.g., $^{13}C^{\alpha}$ and $^{13}C'$). The residues showing a mutation-specific exchange in A4V are part of the N-terminal protecting edge of the β-sheet that is stable in WT (β1–3 and β6; Fig. 3*B*). The destabilization of β1 in the excited state of A4V implies exposure of β2, which shows high intrinsic propensity for fibril formation (32). G85R affects residues in β6 and loop V, which together form the C-terminal protective edge of the β-sheet (Fig. 3*C*), as well as in β3 next to β6. The D90A mutation affects loop V and the adjacent loop III (Fig. 3*D*). In addition, β4 and β7 appear to be perturbed in A4V and D90 beyond what is observed in WT.

Discussion

Here, we have demonstrated that monomeric apo-SOD1 exchanges between the globular folded state and an excited state

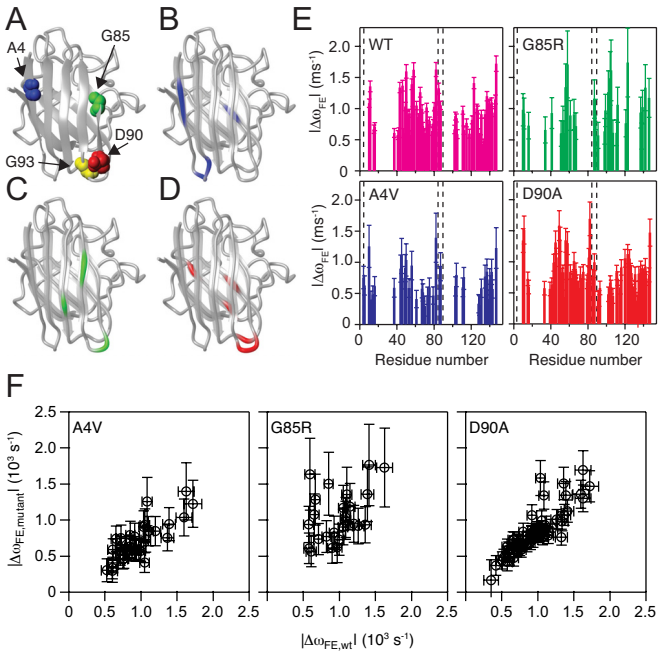

Fig. 3. Structural variation between the excited states of WT and mutant variants of apo-SOD1. (*A*) Structural location of the mutated residues in the SOD1 variants investigated herein. Blue, A4; green, G85; red, D90; yellow, G93. (*B–D*) The locations of residues that are perturbed in the excited state of the mutants, but not in WT apo-SOD1. (*B*) A4V: residues 4–6 (located in β1), 12 and 14 (loop I), and 45 (β4). (*C*) G85R: residues 34 (β3), 91 (loop V), and 98–99 (β6). (*D*) D90A: residues 39 (loop III), 45 (β4), 91–92 (loop V), 116 and 120 (β7). (*E*) Differences in the chemical shifts of the backbone amide ^{15}N nuclei between the exchanging folded and excited states, obtained from CPMG relaxation dispersions. The magnitude of the chemical shift change, $\Delta\omega_{FE}$, is plotted versus residue number. The dashed lines indicate the locations of the mutated residues. The color code is as in (*A*)–(*D*). (*F*) The $\Delta\omega_{FE}$ values obtained for each of the mutants plotted versus $\Delta\omega_{FE}$ for WT SOD1. The Pearson correlation coefficient, *r*, and *P* values are as follows: A4V versus WT, $r = 0.80$ and $P < 0.0001$; G85R versus WT, $r = 0.41$ and $P = 0.039$; D90A versus WT, $r = 0.86$ and $P < 0.0001$.

that forms nonnative intermolecular interactions. That fact that regions of apo-SOD1 are highly dynamic has been recognized for years (25), but it is not clear whether the observed variables, such as NMR relaxation rates and amide hydrogen exchange with solvent deuterium (18, 19, 25, 33), imply that SOD1 experiences a conformational continuum within a single basin in the energy landscape, large-scale unfolding of the affected regions, or exchange to a relatively well-defined excited state. Our present results provide evidence for the latter scenario, and further show that the excited state is a unifying feature of all SOD1 variants investigated herein, despite their significant variation in stability toward global unfolding. Under the present experimental conditions, we could not obtain any CPMG dispersion data on the folded state of the G93A mutant due to its low population. Thus, it remains to be investigated whether the folded states of G93A and other severely destabilized mutants also exhibit the transient conformational distortion observed for the other 4 variants.

Our data reveal molecular properties of SOD1 that may offer insight into the variations in disease propensity and progression observed among different mutants. Previous reports have shown that the net electric charge of SOD1 mutants is an important factor in ALS (14, 28). Because the population of monomeric apo-SOD1 depends on a number of factors, including dimer interface integrity, metal affinity, and disulfide oxidation state, mutations compromising any of these properties would be expected to influence disease propensity (2, 11). Cellular properties, including dysfunction of the chaperone and proteasome systems, also are predicted to play a role in the development of ALS (1). Below we discuss structural and physicochemical properties of the excited state that are likely to influence the aberrant oligomerization of SOD1.

The $\Delta\omega_{FE}$ values indicate a significant structural change between the folded and excited states, yet the values of $\Delta\omega_{FE}$ show that the perturbed residues of the excited state do not behave as an unfolded chain (Fig. S4). Given that the excited state is destabilized ($\Delta G_{FE} = 12$ kJ/mol), this structural change likely involves weakened packing and exposure of hydrophobic side chains that normally are hidden in the protein interior. This interpretation is supported both by the PREs observed for residues that are buried in the ground state and by the temperature dependence of the CPMG data (Fig. 1*B*), which reveals an unfavorable change in entropy, $\Delta S_{FE} = -220$ J/mol/K, as expected for a process that increases the hydrophobic surface area. An upper limit for the change in hydrophobic exposure can be estimated by assuming that ΔS_{FE} is caused entirely by the hydrophobic effect (34), yielding $\Delta A = 635$ Å^2, which is comparable with the surface buried in the highly stable native homodimer ($\Delta A = 660$ Å^2 per monomer) (35, 36). The residues that are perturbed in the excited state do not match those in the native dimer interface (Fig. 1 *A* and *C*), but do match those experiencing PRE (Figs. 1*C* and 2*B*). Thus, we conclude that the excited state constitutes a precursor for nonnative assembly mediated by a structural perturbation that exposes a hydrophobic face capable of association.

Previous observations have indicated that SOD1 oligomers and insoluble aggregates are mediated by amyloid-like interactions between β-strands (11, 15). The present view of the excited state highlights those parts of the monomer that are the most likely to engage in intermolecular β-interactions. Based on the principle that β-sheet edges of native structures oppose aggregation by negative design (37, 38), we note that the perturbation of edge strands β5 and β8 in the excited state makes these regions prime targets for nonnative associations implicated in oligomerization. Indeed, β6 shows PREs due to intermolecular interactions that cannot be explained by the native dimer (Fig. 2*B*) but are made possible by the destabilization of β5 (Fig. 1*B*). Similar observations have been made previously for an amyloid precursor state of β_2-microglobulin (39).

All 3 ALS mutations exhibit additional perturbations of the protective β-sheet edges that remain intact in the excited state of WT apo-SOD1; specifically, this involves strands β1 or β6 or the loops leading into these strands. Consequently, an increased tendency to form nonnative intermolecular interactions is expected for the mutants relative to the WT. The degree of excited-state perturbation follows the rank order of disease severity for the mutants studied here; the excited state of A4V exhibits more critical effects than either of G85R or D90A, because it exposes β2, which has a high propensity for fibril formation (32). These observations suggest that structural differences between the excited states of different SOD1 variants may be a critical factor in determining oligomerization propensities and disease progression.

Do the kinetic and thermodynamic properties of the excited states reveal any further determinants of variations in disease severity? The populations of the excited states differ by less than a factor of 2 between the WT and mutant variants. Nevertheless, p_E, which is expected to scale the effective rate of oligomerization, appears to be slightly greater for some mutants than for WT. The same observation holds for the exchange rate, indicating that the energy barrier between the folded and excited states is reduced by mutations (Table 1). Although the observed changes in p_E are limited, we note that even smaller changes ($< 15\%$) in the aggregation propensity of Alzheimer's β-peptide produce profound changes in its pathogenic effects (40). It would

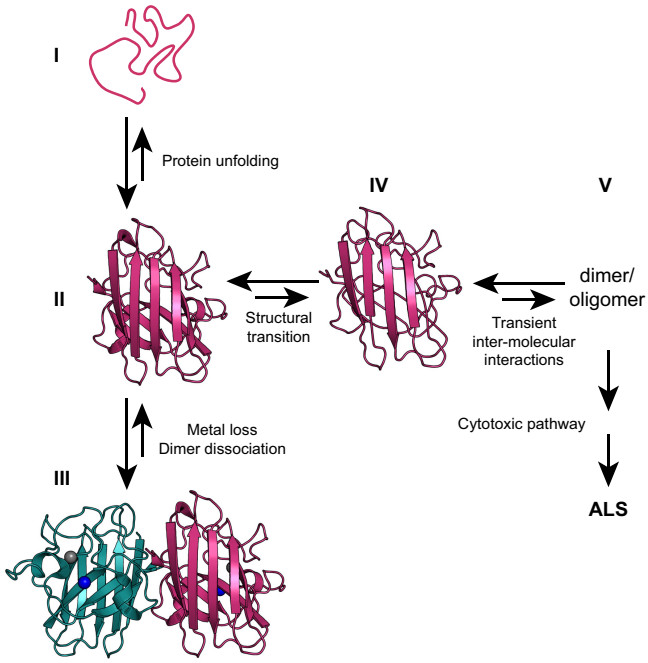

Fig. 4. Schematic diagram of the initial molecular events triggering aberrant oligomerization of apo-SOD1. (*I*) Unfolded apo-SOD1. (*II*) Folded ground state of monomeric apo-SOD1. (*III*) Native dimeric Cu/Zn-bound SOD1. (*IV*) Excited state of monomeric apo-SOD1 with destabilized edge β-strands and increased hydrophobic surface area. The excited state defines the gateway to oligomerization implicated in ALS. (*V*) Nonnative dimer or oligomer. Arrows indicate equilibria; the relative size of the arrows qualitatively depicts the balance across each equilibrium, which depends on the specific mutation, among other things.

be of great interest to compare our results with measured rates of oligomerization or aggregation for the same SOD1 variants. But to the best of our knowledge, this type of data has not yet been published, although qualitative results have been reported for WT and D90A (41). At present, we can only speculate that the differences in p_E and k_{ex} between SOD1 variants (up to 70% in the present cases), in combination with the structural differences between their excited states, might represent important factors underlying the variations in development and progression of ALS observed for different mutations.

We note that the detailed view of the excited state provided here differs from that inferred from previous ϕ-value analysis of the folding kinetics (42), possibly suggesting that the excited state is off the folding pathway; alternatively, the observed differences arguably could be explained by the limited structural resolution afforded by the ϕ-value approach. The chemical shifts of the perturbed residues in the excited state suggest that the protein is not simply undergoing local unfolding, which implies that the approach reported by Korzhnev et al. (43) toward calculating the structure of the excited state cannot be applied in the present case, because one of the endpoint reference states remains unknown.

Our current model of the initial steps that lead to aberrant oligomerization of SOD1 is summarized in Fig. 4. The critical event is the reversible transition of apo-SOD1, in either the disulfide-oxidized or disulfide-reduced state, to a destabilized conformation that forms nonnative oligomers. We hypothesize that this transition might constitute the gateway to downstream events leading to ALS. The excited state is a unifying factor among ALS-associated SOD1 mutations with widely differing physicochemical properties, including global stability. Our model implies that WT SOD1 also is able to form oligomers, although with decreased probability. This inherent feature explains the observations that WT SOD1 can oligomerize or aggregate (11, 15, 16), that inclusions of WT SOD1 have been identified in patients with sporadic ALS (7), and that WT SOD1 exacerbates disease in double-transgenic mice (44). The initial misfolding transition of SOD1 might serve as a target for intervention of SOD1-associated cytotoxicity in ALS.

Materials and Methods

Protein Expression and Purification. The previously validated mutant C6A/F50E/G51E/C111A was used as a substitute for monomeric WT SOD1 (14), because it enables studies of the monomer under equilibrium conditions and avoids nonnative disulfide cross-linking of C6 and C111, which compromises the long-term solubility required for the NMR analysis. All of the ALS mutations studied here were expressed on the background of this pseudo-WT construct, designated WT herein. The WT and A4V, G85R, D90A, and G93A mutants were expressed as described in ref. 14 in *Escherichia coli* strains BL21(DE3) or BL21*(DE3)/pLysS. The mutant Q153C was constructed using the Quick Change Lightning site-directed mutagenesis kit (Stratagene), with the WT construct as a template. Unlabeled SOD1 was expressed in LB medium. SOD1 enriched with ^{15}N and ^{13}C was expressed in M9 minimal medium containing $^{15}NH_4Cl$ and [U-$^{13}C_6$]-Glc as the sole nitrogen and carbon sources. The protein was purified essentially as described in ref. 14. Spin-labeled SOD1-Q153C was prepared in N_2-flushed 20 mM Tris·HCl (pH 8.0) by mixing with 6 molar equivalents of MTSL. The sample was placed in the dark at 25 °C for 1–1/2 hours, followed by dialysis against 10 mM Tris·HCl (pH 8.0) at 5 °C. Unlabelled protein was removed using MonoQ anion exchange with a 0–0.25 M NaCl elution gradient in 20 mM Tris·HCl (pH 8.0).

NMR Sample Preparation. All NMR samples were made up in 10 mM MES, pH 6.3, 10% D_2O, and 1 mM EDTA, unless stated otherwise. Apo-SOD1 was prepared by extensive dialysis against 50 mM NaAcO and 10 mM EDTA (pH 3.8), followed by dialysis against the NMR buffer and concentration to 0.25–1 mM. Reduced apo-SOD1 was prepared by adding 50 mM DTT to an Ar-purged solution of apo-SOD1 in 20 mM Tris (pH 8), incubation under Ar atmosphere for 2 h at 37 °C, and buffer exchange to yield 0.8 mM reduced apo-SOD1 with 0.5 mM tris(2-carboxyethyl)phosphine. Zn-SOD was prepared by 10-fold dilution of 1 mM apo-SOD into 0.5 mM $ZnCl_2$ without EDTA, and concentration to 1 mM. The sample for paramagnetic relaxation measurements was prepared by mixing 60 μL of 1 mM ^{15}N apo-SOD1 with 540 μL of 1 mM apo-Q153C-MTSL.

NMR Experiments. Backbone resonances for WT SOD1, A4V, and G85R were assigned using ^1H-^{15}N HSQC, HNCO, HNCA, (HCA)CO(CA)NH, HNCACB, and CBCA(CO)NH experiments (45). The WT assignments could be transferred to D90A using a single HNCA spectrum. ^{15}N CPMG relaxation-compensated experiments (46) were performed using the constant time approach (47) on Varian Inova 500 and 600 MHz spectrometers equipped with triple-resonance probes. All spectra were processed in nmrPipe (48) and analyzed with nmrDraw and SPARKY 3. CPMG dispersions were measured at 18, 25, and 32 °C on WT SOD1 and at 25 °C on the A4V, G85R, and D90A mutants. Dispersion profiles were sampled using 17 CPMG field strengths (ν_{CPMG}) ranging from 50 to 1,000 Hz at 11.7 T and 14 values of ν_{CPMG} ranging from 33 to 1,000 Hz at 14.1 T; $\nu_{CPMG} = 1/(4\tau_{CPMG})$, where $2\tau_{CPMG}$ is the spacing between 2 successive 180° pulses in the CPMG pulse train. ^1H Γ_2 experiments were recorded using a published pulse sequence (31) on a Varian Inova 800 spectrometer with a triple-resonance cryoprobe. Relaxation decays were measured before and after reduction of the MTSL spin-label with 3 molar excess ascorbate, using 8 relaxation delays of 2–40 ms.

Data Analysis. Relaxation dispersion profiles on apo-SOD1 were fitted both to a constant value and to the general expression for a 2-state process (49). Relaxation dispersion profiles on Zn-SOD1 were fitted to a constant and the expression for a 2-state process in slow exchange (50). The van't Hoff equation was applied to model the temperature dependence of p_F, while k_{ex} was fit individually at each temperature to allow for non-Arrhenius dynamics. The *F* test was used to determine whether each residue showed significant dispersions (51, 52). For the single-temperature data, $P < 0.02$ was used as significance criterion. For the 3-temperature data, $P < 0.0005$ was used to ensure convergence of the global fit, which resulted in selection of essentially the same residues as those identified from single-temperature data and $P < 0.02$. Data from residues with significant dispersion were subsequently included in a global fit with k_{ex} and p_F as global parameters. Global fits were performed using IgorPro v5.04 (WaveMetrics). To assess the robustness and quality of the global fit, a bootstrap procedure was used; 20% of the residues with signifi-

cant dispersion were randomly left out in 100 repeated global fits. To test whether the parameters p_F and k_{ex} differ between the WT and mutants, data were fit pairwise with either p_F or k_{ex} as a parameter shared between the WT and mutant. The results of these fits were compared with the fits of each SOD variant treated individually by applying the *F* test. Γ_2 was measured from intensity profiles profiles as described in ref. 31. Data were fitted both to a constant and to an exponential decay, and the *F* test was used to determine whether Γ_2 was significant ($P < 0.01$). The PREs expected for the native dimer were calculated as described in ref. 31, based on a correlation time of 10 ns (25). The distance between each amide proton and the unpaired electron of MTSL was estimated from the distance between $N^{\epsilon 2}$ of Q153 in WT SOD1 and the amide nitrogen in the dimeric structure of Zn-loaded SOD1, PDB-code 1HL4 (35).

ACKNOWLEDGMENTS. This work was funded by the Göran Gustafsson Foundation for Research in Natural Sciences and Medicine (M.A.), the Swedish Research Council (M.A. and M.O.), the Knut and Alice Wallenberg Foundation (M.A.), the Carl Tryggers Stiftelse för Vetenskaplig Forskning (M.A.), an EMBO postdoctoral fellowship and the Danish Natural Science Research Council Grant 272-060251 (to K.T.), and a Fulbright Research grant (to M.H.S.).

1. Pasinelli P, Brown RH (2006) Molecular biology of amyotrophic lateral sclerosis: Insights from genetics. *Nat Rev Neurosci* 7:710–723.
2. Valentine JS, Doucette PA, Potter SZ (2005) Copper-zinc superoxide dismutase and amyotrophic lateral sclerosis. *Annu Rev Biochem* 74:563–593.
3. Gurney ME, et al. (1994) Motor neuron degeneration in mice that express a human Cu,Zn superoxide-dismutase mutation. *Science* 264:1772–1775.
4. Bruijn LI, et al. (1998) Aggregation and motor neuron toxicity of an ALS-linked SOD1 mutant independent from wild-type SOD1. *Science* 281:1851–1854.
5. Johnston JA, Dalton MJ, Gurney ME, Kopito RR (2000) Formation of high molecular weight complexes of mutant Cu,Zn-superoxide dismutase in a mouse model for familial amyotrophic lateral sclerosis. *Proc Natl Acad Sci USA* 97:12571–12576.
6. Jonsson PA, et al. (2004) Minute quantities of misfolded mutant superoxide dismutase-1 cause amyotrophic lateral sclerosis. *Brain* 127:73–88.
7. Gruzman A, et al. (2007) Common molecular signature in SOD1 for both sporadic and familial amyotrophic lateral sclerosis. *Proc Natl Acad Sci USA* 104:12524–12529.
8. Karch CM, Prudencio M, Winkler DD, Hart PJ, Borchelt DR (2009) Role of mutant SOD1 disulfide oxidation and aggregation in the pathogenesis of familial ALS. *Proc Natl Acad Sci USA* 106:7774–7779.
9. Chiti F, Dobson CM (2009) Amyloid formation by globular proteins under native conditions. *Nat Chem Biol* 5:15–22.
10. Rakhit R, Chakrabartty A (2006) Structure, folding, and misfolding of Cu,Zn superoxide dismutase in amyotrophic lateral sclerosis. *Biochim Biophys Acta* 1762:1025–1037.
11. Furukawa Y, Kaneko K, Yamanaka K, O'Halloran TV, Nukina N (2008) Complete loss of post-translational modifications triggers fibrillar aggregation of SOD1 in the familial form of amyotrophic lateral sclerosis. *J Biol Chem* 283:24167–24176.
12. Rakhit R, et al. (2004) Monomeric Cu,Zn-superoxide dismutase is a common misfolding intermediate in the oxidation models of sporadic and familial amyotrophic lateral sclerosis. *J Biol Chem* 279:15499–15504.
13. Khare SD, Caplow M, Dokholyan NV (2004) The rate and equilibrium constants for a multistep reaction sequence for the aggregation of superoxide dismutase in amyotrophic lateral sclerosis. *Proc Natl Acad Sci USA* 101:15094–15099.
14. Lindberg MJ, Byström R, Boknäs N, Andersen PM, Oliveberg M (2005) Systematically perturbed folding patterns of amyotrophic lateral sclerosis (ALS)-associated SOD1 mutants. *Proc Natl Acad Sci USA* 102:9754–9759.
15. Banci L, et al. (2007) Metal-free superoxide dismutase forms soluble oligomers under physiological conditions: A possible general mechanism for familial ALS. *Proc Natl Acad Sci USA* 104:11263–11267.
16. Chattopadhyay M, et al. (2008) Initiation and elongation in fibrillation of ALS-linked superoxide dismutase. *Proc Natl Acad Sci USA* 105:18663–18668.
17. Ding F, Dokholyan NV (2008) Dynamical roles of metal ions and the disulfide bond in Cu,Zn superoxide dismutase folding and aggregation. *Proc Natl Acad Sci USA* 105:19696–19701.
18. Banci L, et al. (2009) Structural and dynamic aspects related to oligomerization of apo SOD1 and its mutants. *Proc Natl Acad Sci USA* 106:6980–6985.
19. Nordlund A, et al. (2009) Functional features cause misfolding of the ALS-provoking enzyme SOD1. *Proc Natl Acad Sci USA* 106:9667–9672.
20. Rakhit R, et al. (2007) An immunological epitope selective for pathological monomer-misfolded SOD1 in ALS. *Nat Med* 13:754–759.
21. Bruns CK, Kopito RR (2007) Impaired post-translational folding of familial ALS-linked Cu,Zn superoxide dismutase mutants. *EMBO J* 26:855–866.
22. Arnesano F, et al. (2004) The unusually stable quaternary structure of human Cu,Zn-superoxide dismutase 1 is controlled by both metal occupancy and disulfide status. *J Biol Chem* 279:47998–48003.
23. Cozzolino M, et al. (2007) Cysteine 111 affects aggregation and cytotoxicity of mutant Cu,Zn-superoxide dismutase associated with familial amyotrophic lateral sclerosis. *J Biol Chem* 283:866–874.
24. Niwa J, et al. (2007) Disulfide bond mediates aggregation, toxicity, and ubiquitylation of familial amyotrophic lateral sclerosis–liked mutant SOD1. *J Biol Chem* 282:28087–28095.
25. Banci L, Bertini I, Cramaro F, Del CR, Viezzoli MS (2003) Solution structure of Apo Cu,Zn superoxide dismutase: Role of metal ions in protein folding. *Biochemistry* 42:9543–9553.
26. Palmer AG, Kroenke CD, Loria JP (2001) Nuclear magnetic resonance methods for quantifying microsecond-to-millisecond motions in biological macromolecules. *Methods Enzymol* 339:204–238.
27. Mittermaier A, Kay LE (2006) New tools provide new insights in NMR studies of protein dynamics. *Science* 312:224–228.
28. Sandelin E, Nordlund A, Andersen PM, Marklund SL, Oliveberg M (2007) Amyotrophic lateral sclerosis–associated copper/zinc superoxide dismutase mutations preferentially reduce the repulsive charge of the proteins. *J Biol Chem* 282:21230–21236.
29. Schubert M, Labudde D, Oschkinat H, Schmieder P (2002) A software tool for the prediction of Xaa–Pro peptide bond conformations in proteins based on C-13 chemical shift statistics. *J Biomol NMR* 24:149–154.
30. Wang Y, Jardetzky O (2002) Investigation of the neighboring residue effects on protein chemical shifts. *J Am Chem Soc* 124:14075–14084.
31. Iwahara J, Tang C, Clore GM (2007) Practical aspects of H-1 transverse paramagnetic relaxation enhancement measurements on macromolecules. *J Magn Reson* 184:185–195.
32. Rousseau F, Schymkowitz J, Oliveberg M (2008) ALS precursor finally shaken into fibrils. *Proc Natl Acad Sci USA* 105:18649–18650.
33. Rodriguez JA, et al. (2005) Destabilization of apoprotein is insufficient to explain Cu,Zn-superoxide dismutase-linked ALS pathogenesis. *Proc Natl Acad Sci USA* 102:10516–10521.
34. Spolar RS, Record MT (1994) Coupling of local folding to site-specific binding of proteins to DNA. *Science* 263:777–784.
35. Strange RW, et al. (2003) The structure of holo and metal-deficient wild-type human Cu, Zn superoxide dismutase and its relevance to familial amyotrophic lateral sclerosis. *J Mol Biol* 328:877–891.
36. Elam JS, et al. (2003) Amyloid-like filaments and water-filled nanotubes formed by SOD1 mutant proteins linked to familial ALS. *Nat Struct Biol* 10:461–467.
37. Otzen DE, Kristensen O, Oliveberg M (2000) Designed protein tetramer zipped together with a hydrophobic Alzheimer homology: A structural clue to amyloid assembly. *Proc Natl Acad Sci USA* 97:9907–9912.
38. Richardson JS, Richardson DC (2002) Natural β-sheet proteins use negative design to avoid edge-to-edge aggregation. *Proc Natl Acad Sci USA* 99:2754–2759.
39. Jahn TR, Parker MJ, Homans SW, Radford SE (2006) Amyloid formation under physiological conditions proceeds via a native-like folding intermediate. *Nat Struct Mol Biol* 13:195–201.
40. Luheshi LM, et al. (2007) Systematic in vivo analysis of the intrinsic determinants of amyloid b pathogeneicity. *PLOS Biol* 5:2493–2500.
41. Banci L, et al. (2008) SOD1 and amyotrophic lateral sclerosis: Mutations and oligomerzation. *PLoS One* 3:e1677.
42. Nordlund A, Oliveberg M (2006) Folding of Cu/Zn superoxide dismutase suggests structural hotspots for gain of neurotoxic function in ALS: Parallels to precursors in amyloid disease. *Proc Natl Acad Sci USA* 103:10218–10223.
43. Korzhnev DM, et al. (2004) Low-populated folding intermediates of Fyn SH3 characterized by relaxation dispersion NMR. *Nature* 430:586–590.
44. Deng H-X, et al. (2006) Conversion to the amyotrophic lateral sclerosis phenotype is associated with intermolecular linked insoluble aggregates of SOD1 in mitochondria. *Proc Natl Acad Sci USA* 103:7142–7147.
45. Cavanagh J, Fairbrother WJ, Palmer AG, Skelton NJ (1995) *Protein NMR Spectroscopy: Principles and Practice* (Academic, San Diego, CA), p 587.
46. Loria JP, Rance M, Palmer AG (1999) A relaxation-compensated Carr-Purcell-Meiboom-Gill sequence for characterizing chemical exchange by NMR spectroscopy. *J Am Chem Soc* 121:2331–2332.
47. Mulder FAA, Skrynnikov NR, Hon B, Dahlquist FW, Kay LE (2001) Measurement of slow (microseconds-milliseconds) time scale dynamics in protein side chains by 15N relaxation dispersion NMR spectroscopy: Application to Asn and Gln residues in a cavity mutant of T4 lysozyme. *J Am Chem Soc* 123:967–975.
48. Delaglio F, et al. (1995) NMRPipe: A multidimensional spectral processing system based on UNIX pipes. *J Biomol NMR* 6:277–293.
49. Carver JP, Richards RE (1972) A general two-site solution for the chemical exchange produced dependence of T_2 upon the Carr–Purcell pulse separation. *J Magn Reson* 6:89–105.
50. Tollinger M, Skrynnikov NR, Mulder FAA, Forman-Kay JD, Kay LE (2001) Slow dynamics in folded and unfolded states of an SH3 domain. *J Am Chem Soc* 123:11341–11352.
51. Mandel AM, Akke M, Palmer AG (1995) Backbone dynamics of *Escherichia coli* ribonuclease HI: Correlations with structure and function in an active enzyme. *J Mol Biol* 246:144–163.
52. Devore JL (1999) *Probability and Statistics for Engineering and the Sciences* (Brooks/Cole, Monterey, CA), 5th Ed, p 775.